Electronic Supplementary Material (ESI) for Journal of Materials Chemistry A.

Supporting Information

Fluorination promotes lithium salt dissolution in borate esters for lithium metal batteries

Peiyuan Ma,[1] Ritesh Kumar,[1] Minh Canh Vu,[1] Ke-Hsin Wang,[1] Priyadarshini Mirmira,[1] and Chibueze V. Amanchukwu[1*]

[1]Pritzker School of Molecular Engineering, University of Chicago, IL 60637 USA

*Corresponding author

Email: chibueze@uchicago.edu

Table S1. Physical properties of borate ester solvents and electrolytes

	Boiling point at ~5 mbar (°C)*	Melting point (°C)**	Viscosity (mPa·s)
TMEB	82	−13	2.84
TFEB	60	−2	5.12
TMEB 1 M LiFSA	-	-	11.19
TFEB 1 M LiFSA	-	−3	7.85

* Boiling points were measured in fractional distillation.

** Melting points were measured by differential scanning calorimetry (Figure S12).

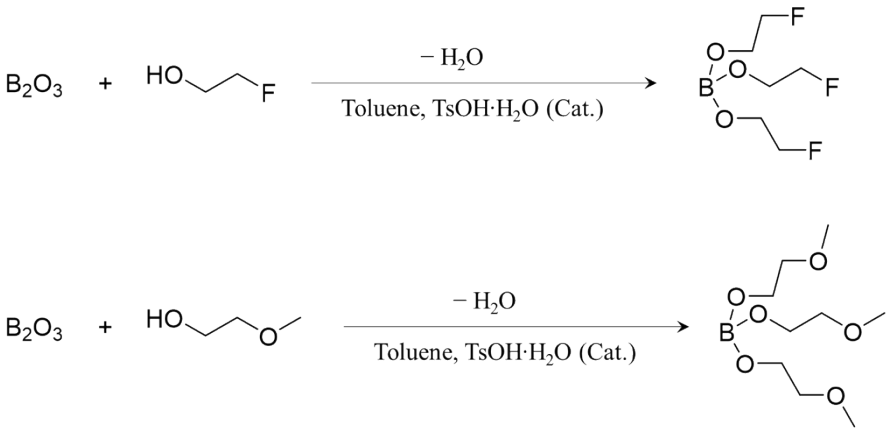

Figure S1. Synthetic route of borate esters.

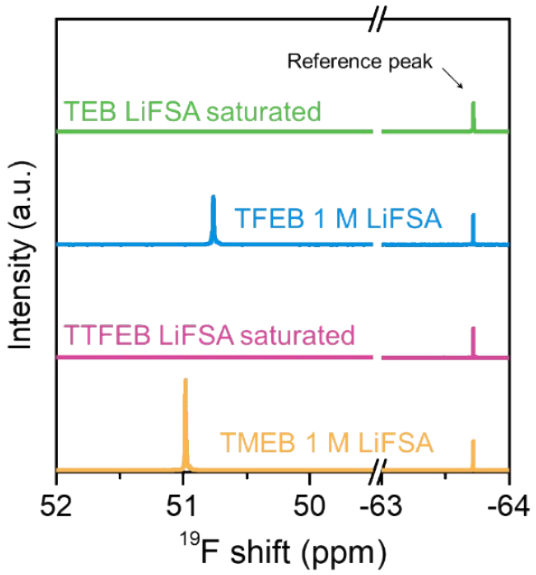

Figure S2. ^{19}F NMR spectra of LiFSA saturated TEB, 1 M LiFSA in TFEB, LiFSA saturated TTFEB and 1 M LiFSA in TMEB. The absence of FSA signal in TEB and TTFEB solutions confirms their poor salt solubility.

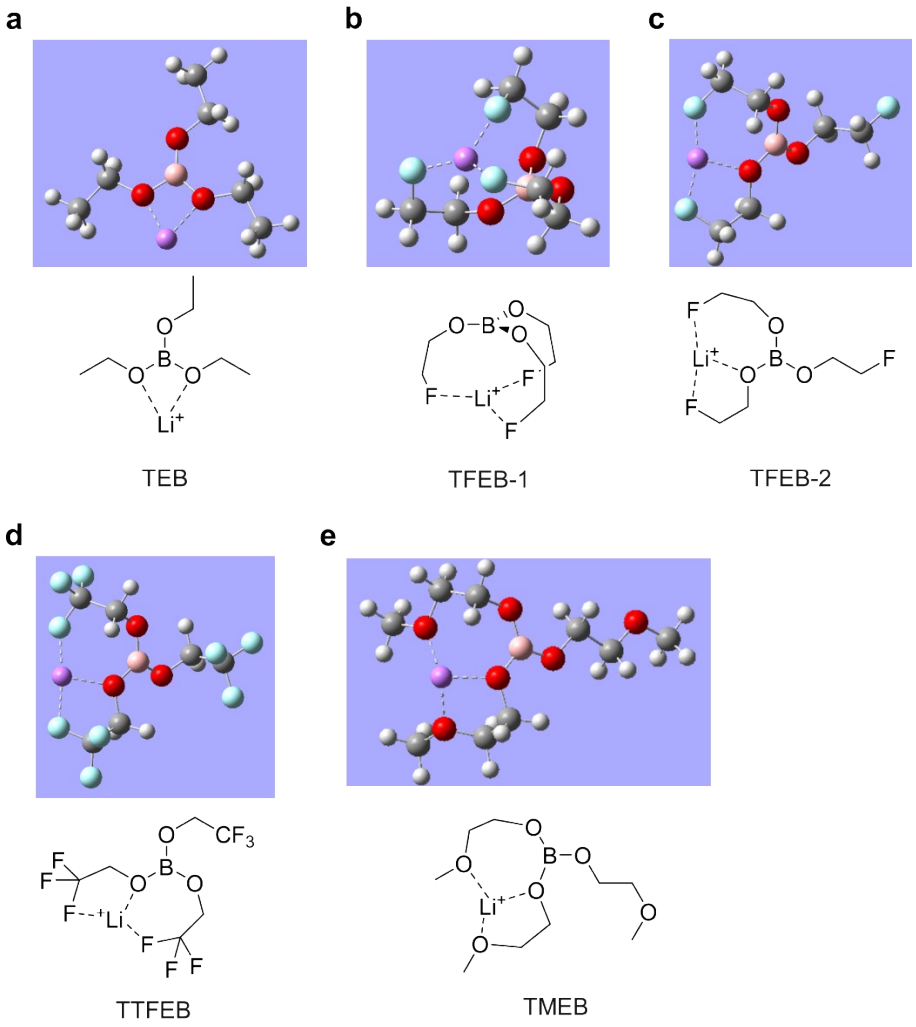

Figure S3. DFT optimized structure of Li^+-solvent pairs: (**a**) TEB; (**b**) Most favorable structure of TFEB; (**c**) Second most favorable structure of TFEB; (**d**) TTFEB; (**e**) TMEB. The solvation energy of TFEB-2 (−98.2 kJ/mol) is slightly higher than TFEB-1 (−103.9 kJ/mol).

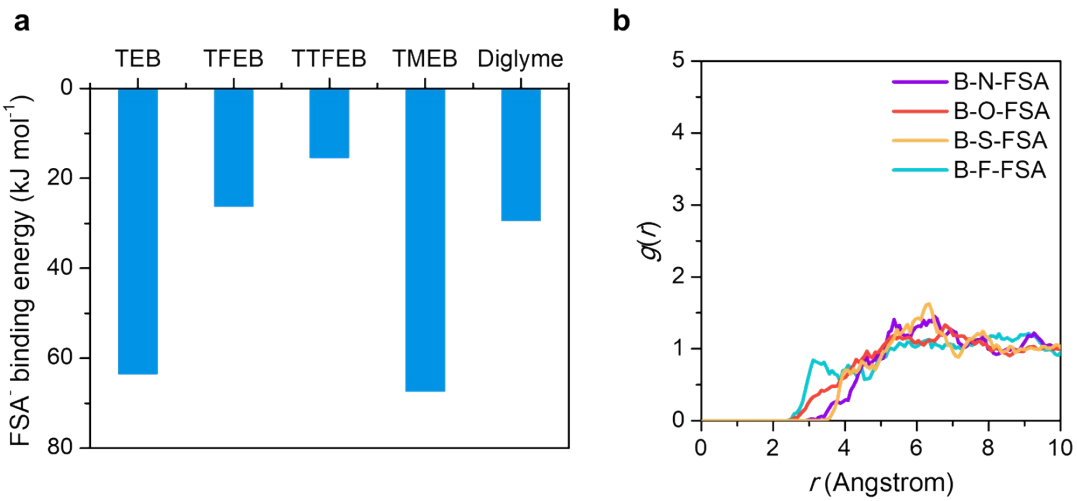

Figure S4. Possibility of anion-solvent coordination. **a**) DFT calculations of binding energy between single solvent molecule and FSA anion, which is defined as G(solvent + FSA^-) − G(solvent) − G(FSA^-). **b**) Radial distribution function (RDF) between boron atom and FSA anion in 1 M LiFSA in TFEB extracted from *ab-initio* molecular dynamics (AIMD) simulation results.

Discussion:

Figure S4a shows the binding energy between solvent and FSA anion predicted by DFT calculations. Surprisingly, TFEB has positive FSA binding energy (26.2 kJ/mol) that is close to diglyme (29.4 kJ/mol), which does not support specific interaction between TFEB and FSA anion. Nonfluorinated borate esters, TEB and TMEB, have even higher binding energy (63.5 kJ/mol and 67.3 kJ/mol) that suggests less favored interaction with FSA anion. Although the more heavily fluorinated TTFEB has slightly lower anion binding energy (15.3 kJ/mol) likely due to stronger electron withdrawing effects of -CF_3 group, the positive binding energy means TTFEB-FSA interaction is still not favored. As shown in Figure S4b, the RDF between boron and FSA extracted from AIMD simulation of 1 M LiFSA in TFEB does not have any obvious peak, which also indicates the lack of specific binding between boron atom and FSA anion. This lack of boron-anion coordination also agrees with the lithium transference number below 0.5 (Figure 3b) because the presence of FSA-solvent coordination should retard anion diffusion and lead to lithium transference number above 0.5.

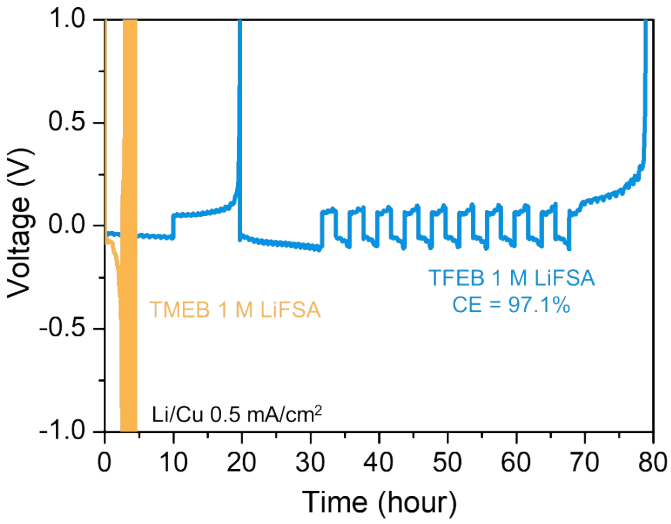

Figure S5. Coulombic efficiency test in lithium metal/copper (Li/Cu) cells using a modified Aurbach protocol at 0.5 mA/cm^2. TFEB 1 M LiFSA maintains high Coulombic efficiency while TMEB electrolyte can barely cycle at 0.5 mA/cm^2.

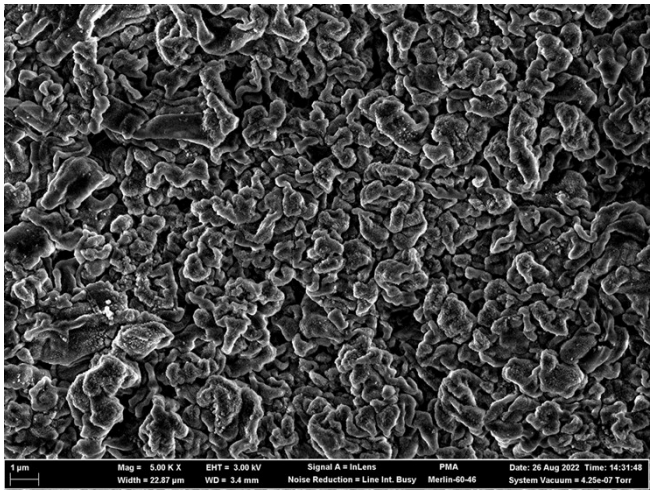

Figure S6. SEM image of lithium deposited in TMEB 1 M LiFSA at a current of 0.1 mA/cm^2 to capacity of 1.5 mAh/cm^2. The morphology of lithium does not change significantly at lower deposition current.

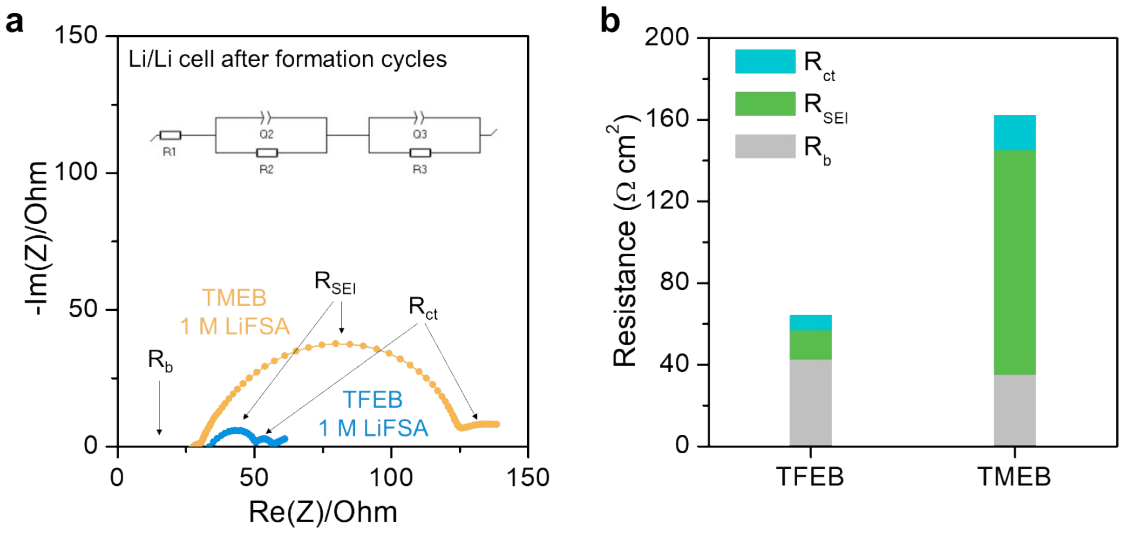

Figure S7. (**a**) Electrochemical impedance spectroscopy (EIS) of Li/Li cells after 5 formation cycles at 0.02 mA/cm^2 to 0.02 mAh/cm^2. The EIS curve is fit with the equivalent circuit shown as inset, where R1, R2 and R3 are assigned to bulk resistance (R_b), SEI resistance (R_{SEI}) and charge transfer resistance (R_{ct}), respectively. (**b**) Contribution of each component to the total resistance of the cell. Resistance values are normalized to geometric area of electrode, 1.13 cm^2. The main difference between TFEB and TMEB appears to be SEI resistance. The much lower SEI resistance of TFEB electrolyte enables better rate capability despite its lower conductivity. Detailed fitting parameters are shown below:

Table S2. EIS fitting parameters

Electrolyte	**R1 (Ω)**	**Q2 (F·s^{a-1})**	**a2**	**R2 (Ω)**	**Q3 (F·s^{a-1})**	**a3**	**R3 (Ω)**
TFEB 1 M LiFSA	37.27	1.319×10^{-8}	0.992	12.78	1.22×10^{-5}	0.871	6.677
TMEB 1 M LiFSA	30.63	1.291×10^{-5}	0.815	97.47	5.74×10^{-3}	1	15.23

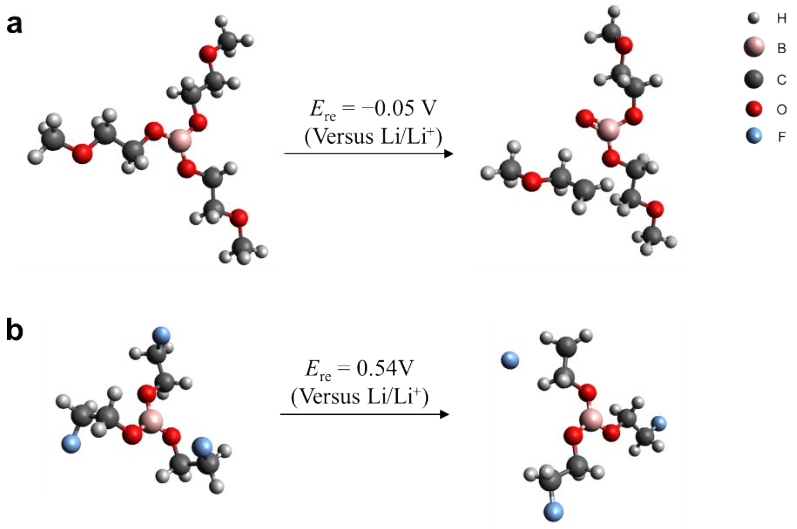

Figure S8. Reductive degradation pathway of (**a**) TMEB and (**b**) TFEB predicted by DFT calculations. TMEB degrades through breaking B-O-C bond while TFEB favors a degradation pathway that breaks C-F bond and eliminates fluoride. The higher reduction potential of TFEB also indicates it can be more easily reduced compared to TMEB.

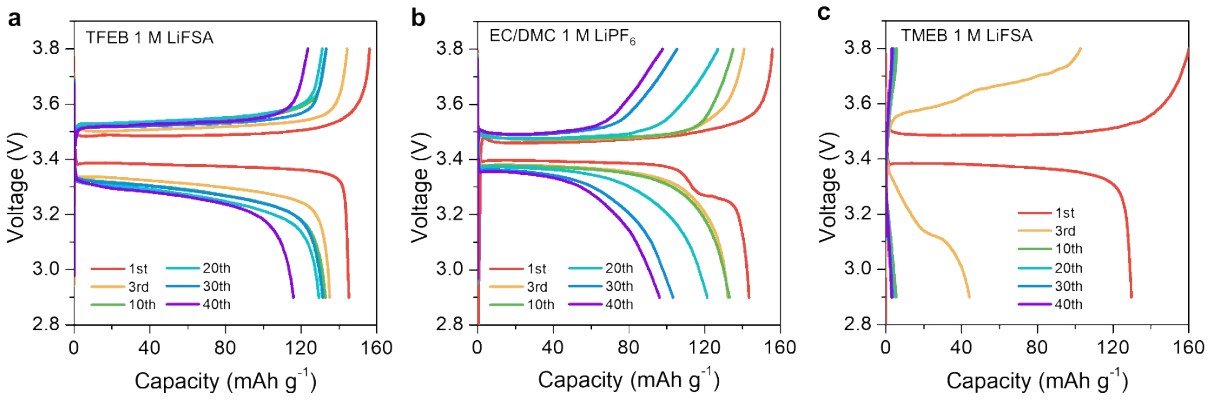

Figure S9. Voltage profiles of 20 μm lithium metal/$LiFePO_4$ (ThinLi/LFP, n/p ≈ 3.2, 1C ≈ 1.81 mA/cm^2) cells using (**a**) 1 M LiFSA in TFEB, (**b**) 1 M $LiPF_6$ in EC/DMC and (**c**) 1 M LiFSA in TMEB. The first two cycles were performed at current rate of C/10 and the following cycles were charged at C/5 and discharged at C/3.

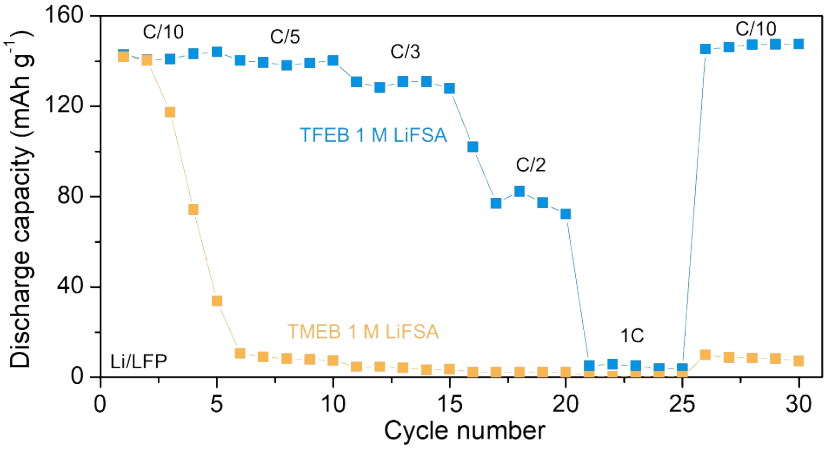

Figure S10. Rate capability test in 375 µm lithium metal/$LiFePO_4$ (Li/LFP) cells. TFEB electrolyte can be cycled up to C/2 while TMEB electrolyte shows rapid capacity decay even at C/10.

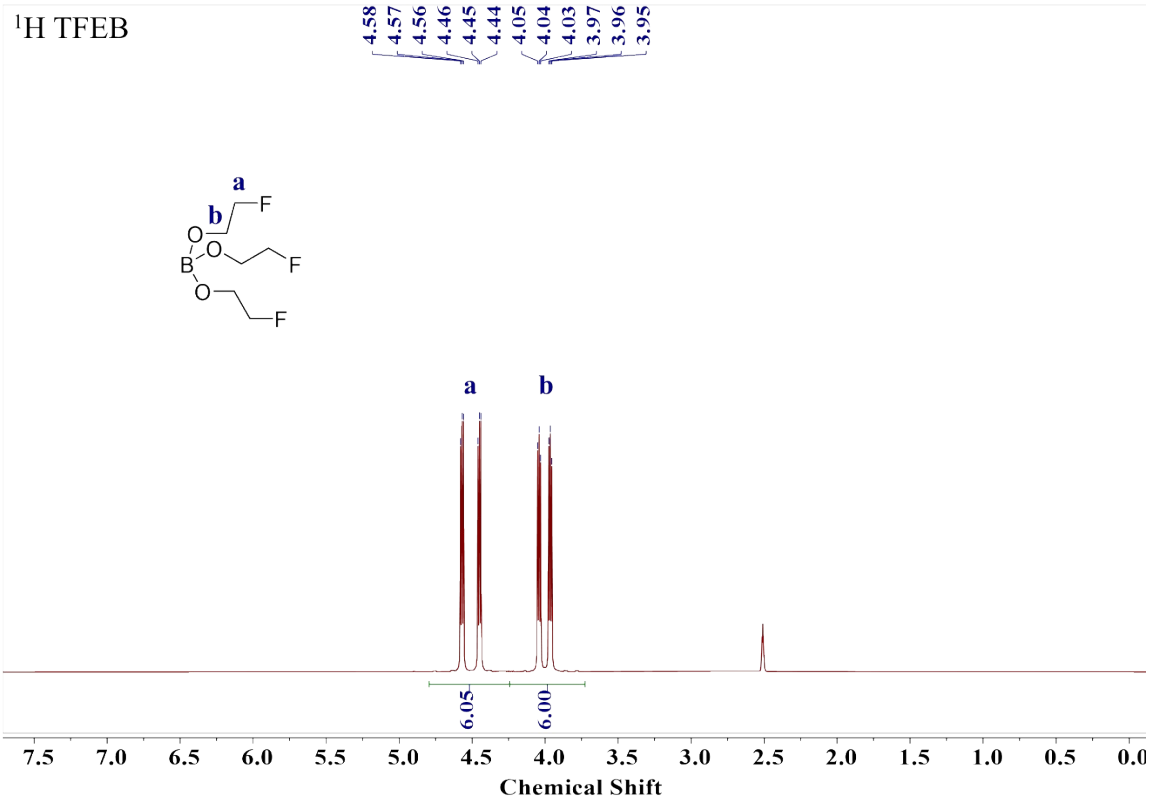
^{1}H TFEB
4.58
4.57
4.56
4.46
4.45
4.44
4.05
4.04
4.03
3.97
3.96
3.95
a
b
F
O
B
O
F
O
F
a
b
6.05
6.00
7.5 7.0 6.5 6.0 5.5 5.0 4.5 4.0 3.5 3.0 2.5 2.0 1.5 1.0 0.5 0.0
Chemical Shift

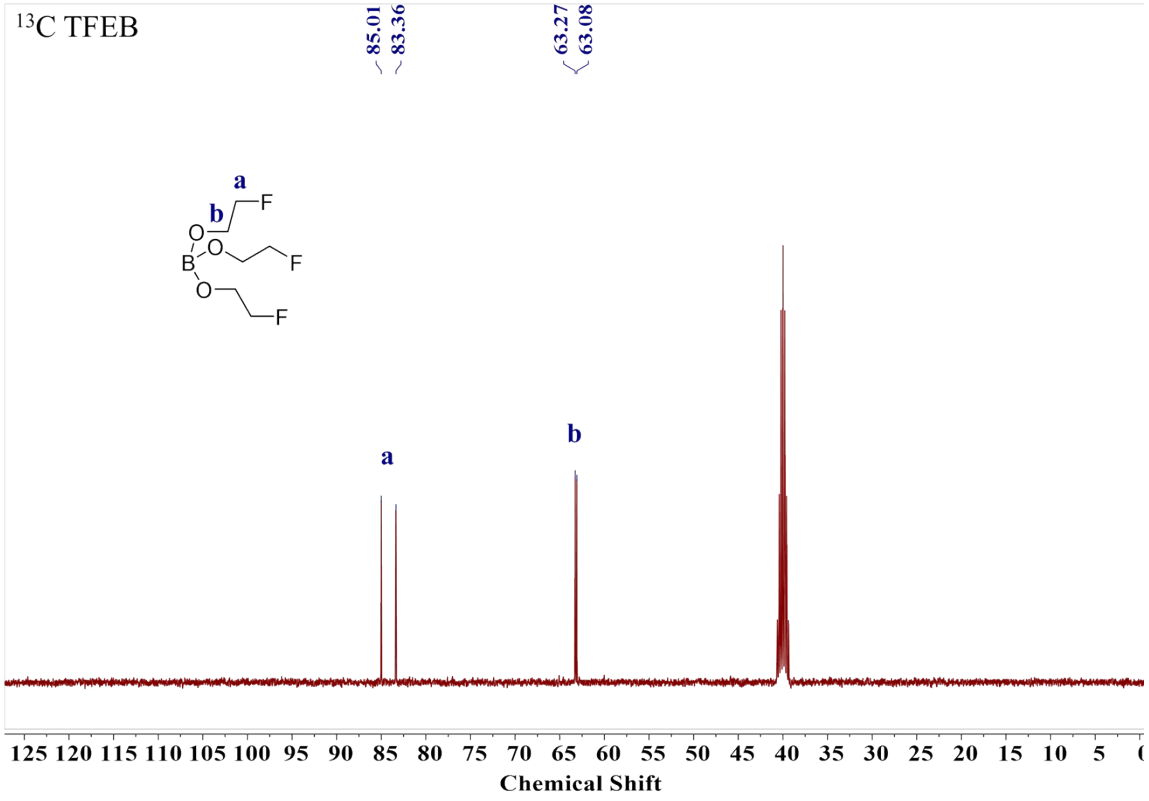
^{13}C TFEB
85.01
83.36
63.27
63.08
a
b
F
O
B
O
F
O
F
a
b
125 120 115 110 105 100 95 90 85 80 75 70 65 60 55 50 45 40 35 30 25 20 15 10 5
Chemical Shift

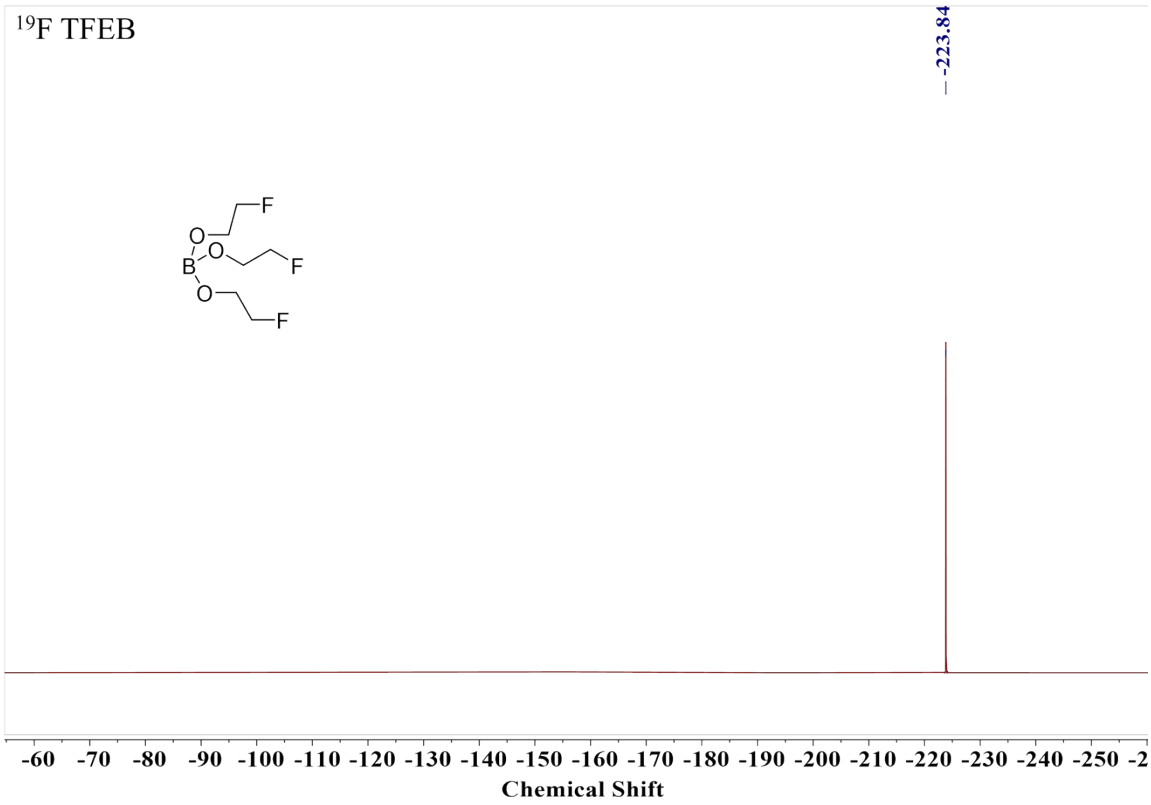
19F TFEB
-223.84
F
O
O
B
O
F
F
-60 -70 -80 -90 -100 -110 -120 -130 -140 -150 -160 -170 -180 -190 -200 -210 -220 -230 -240 -250 -2
Chemical Shift

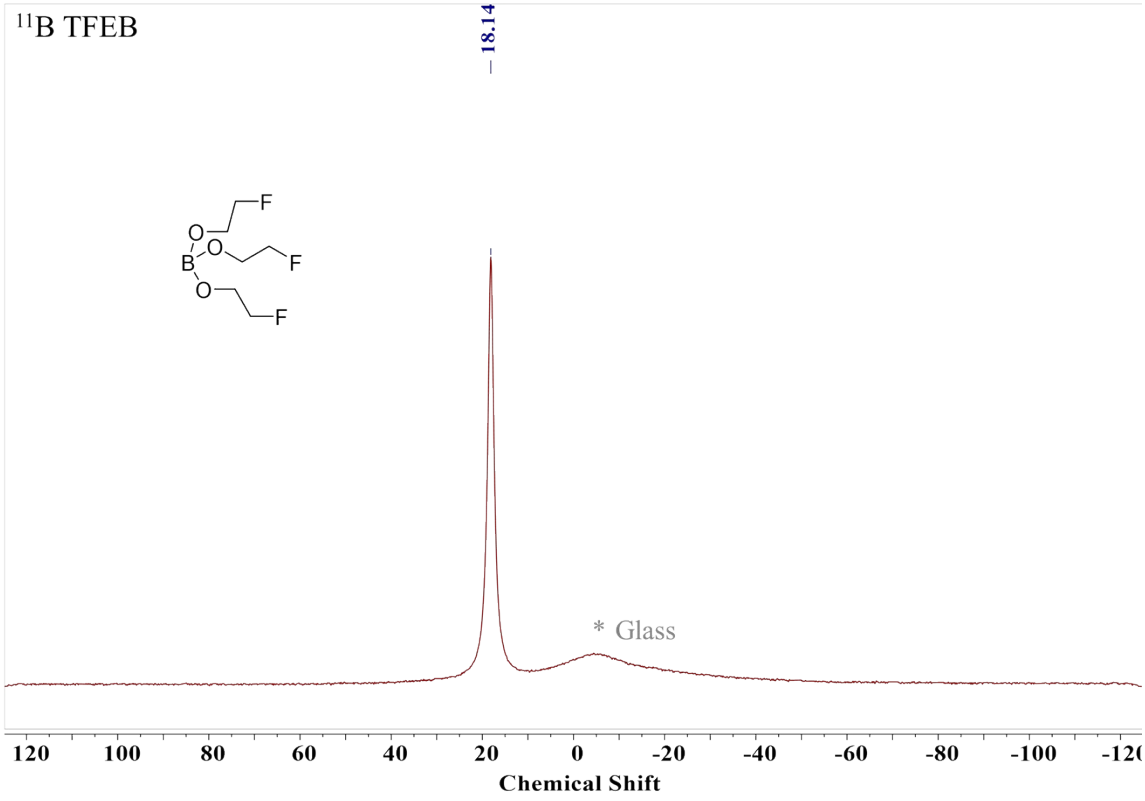
11B TFEB
18.14
F
O
O
B
O
F
F
* Glass
120 100 80 60 40 20 0 -20 -40 -60 -80 -100 -12(
Chemical Shift

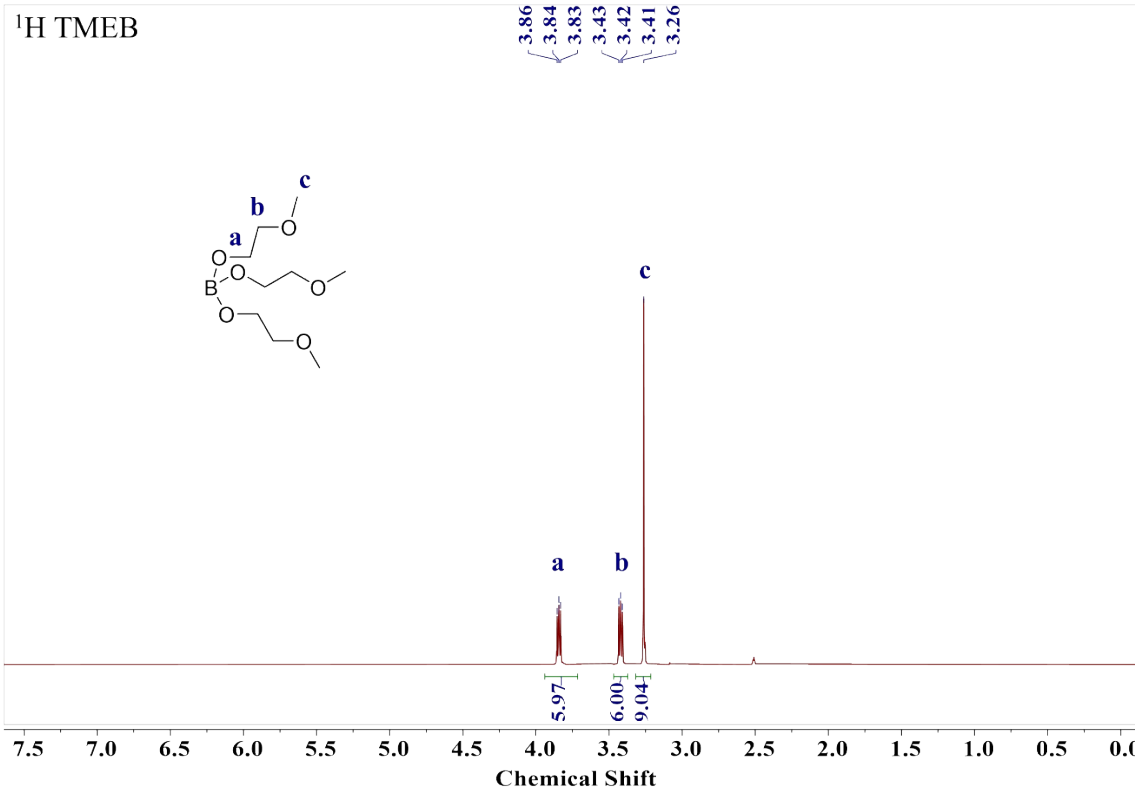
^{1}H TMEB
3.86
3.84
3.83
3.43
3.42
3.41
3.26
a
b
c
5.97
6.00
9.04
7.5 7.0 6.5 6.0 5.5 5.0 4.5 4.0 3.5 3.0 2.5 2.0 1.5 1.0 0.5
Chemical Shift

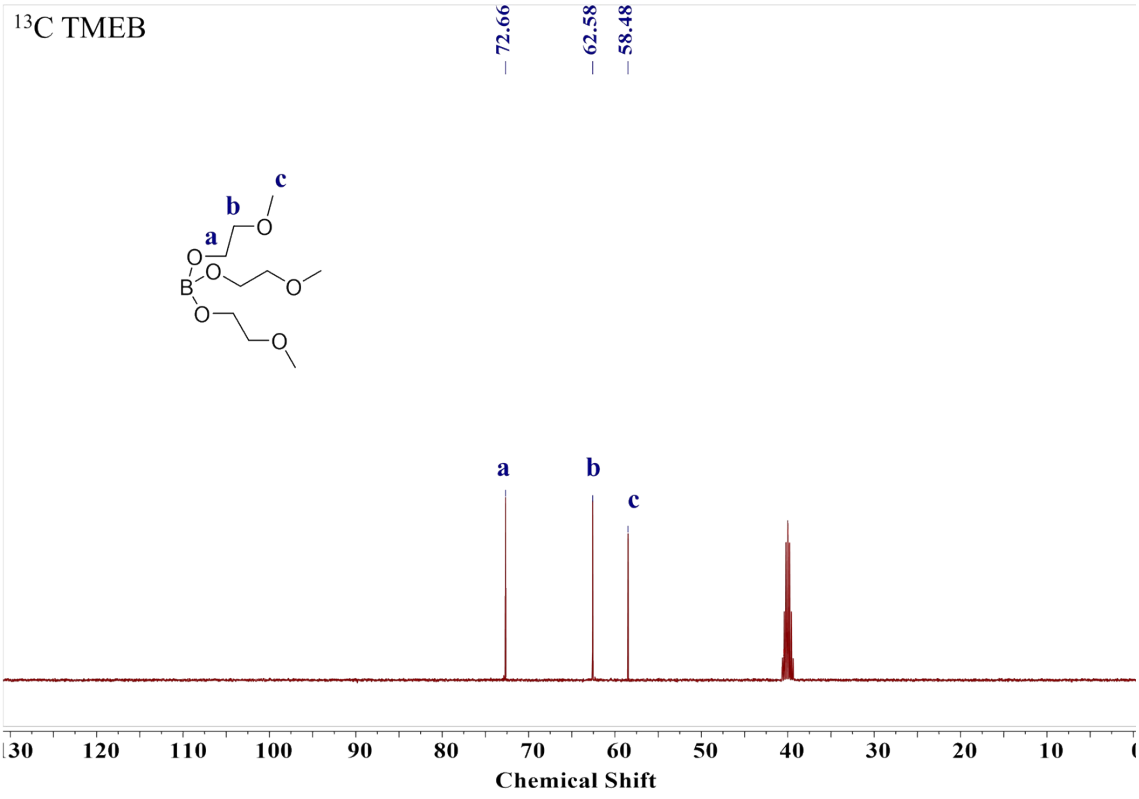
^{13}C TMEB
72.66
62.58
58.48
a
b
c
130 120 110 100 90 80 70 60 50 40 30 20 10
Chemical Shift

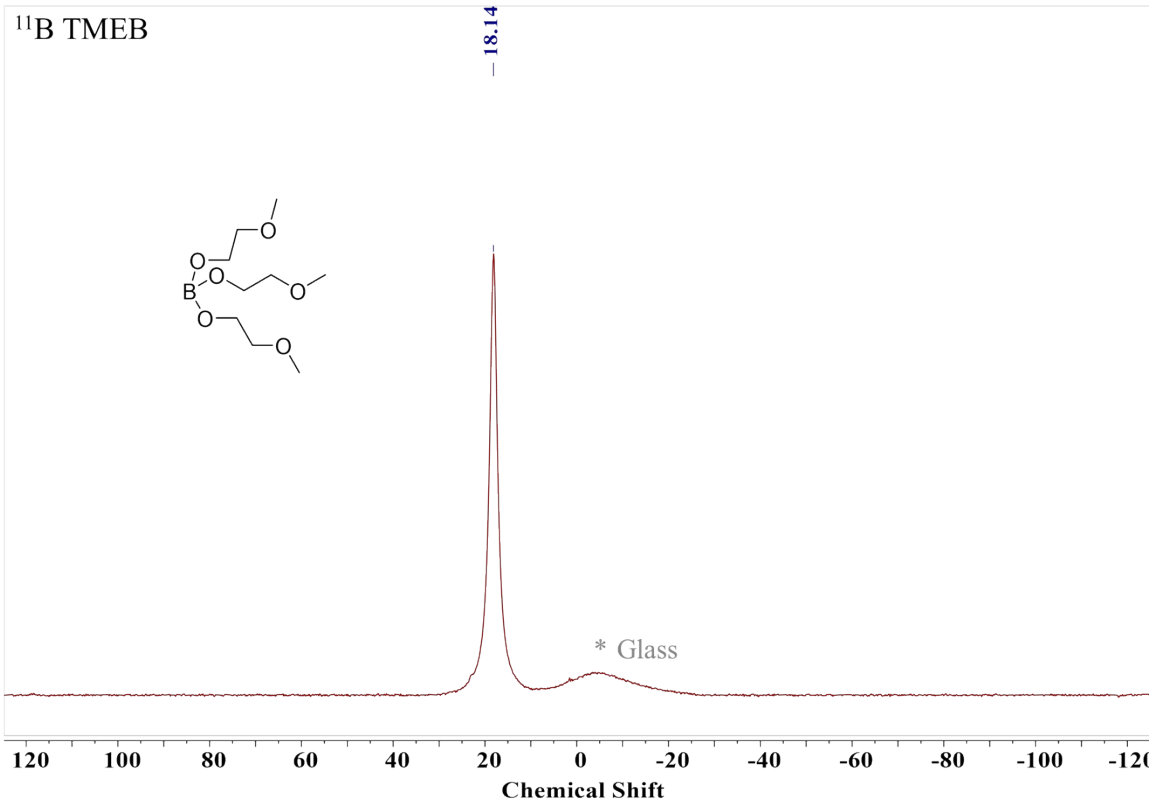

Figure S11. Nuclear magnetic resonance (NMR) spectroscopy of synthesized compounds. ^{1}H, ^{13}C, ^{11}B and ^{19}F (proton decoupled) NMR spectra were taken on a Bruker Ascend 9.4 T / 400 MHz instrument. NMR sample was prepared by dissolving several milligrams of product into 0.5 mL dry D6DMSO inside an argon filled glovebox.

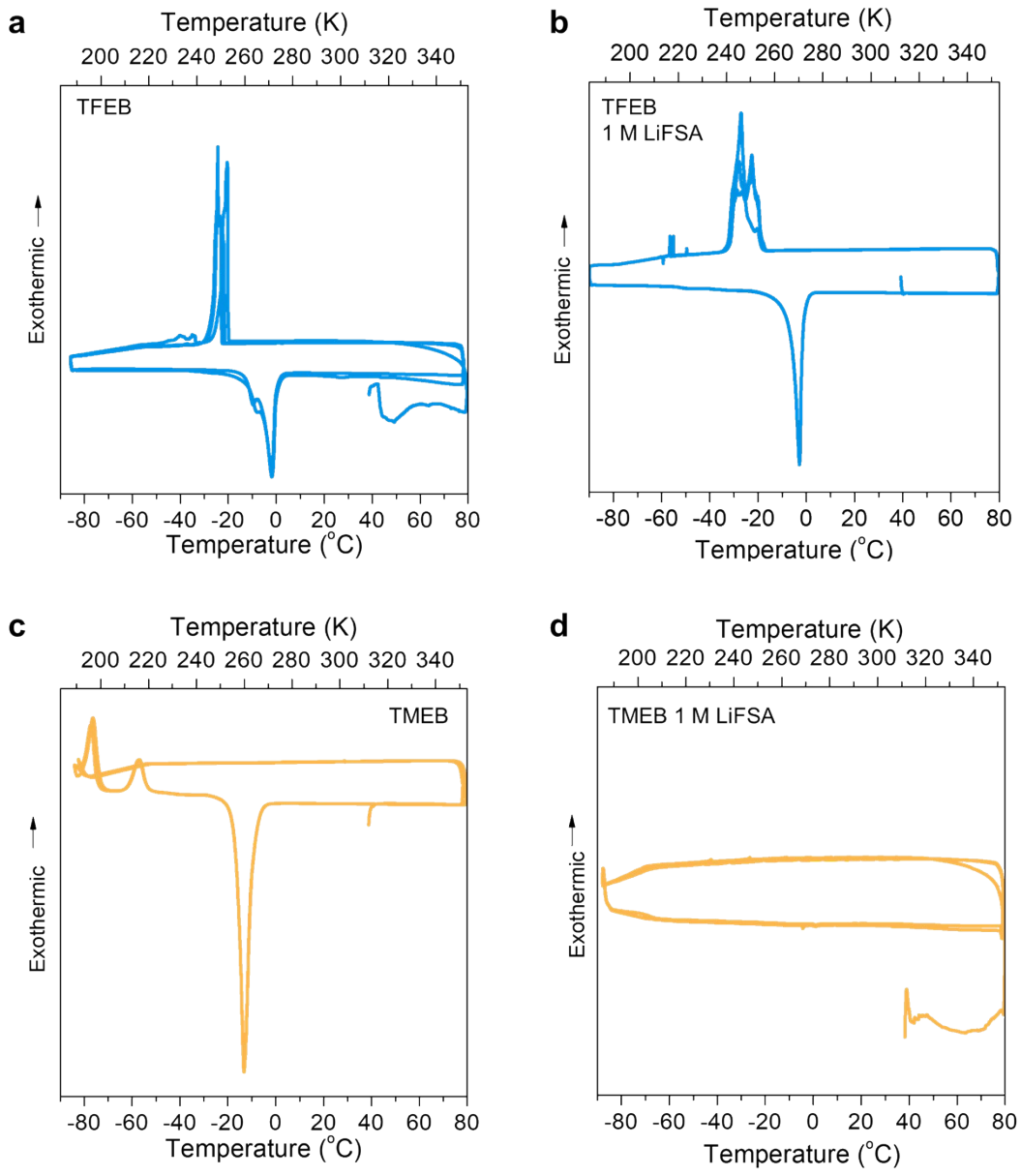

Figure S12. Differential scanning calorimetry (DSC) of borate ester solvents and corresponding electrolytes. (**a**) TFEB solvent has a crystallization transition around −20°C and a melting peak at −2°C. (**b**) 1 M LiFSA in TFEB has a crystallization transition around −27°C and a melting peak at −3°C. (**c**) TMEB solvent has two cold crystallization peaks at −76°C and −57°C and a melting peak at −13°C. (**d**) 1 M LiFSA in TMEB has no obvious thermal transition in the temperature range investigated. DSC was performed with a TA Instruments Discovery 2500 differential scanning calorimeter. Sample was first heated up to 80 °C and then looped between 80 and −90 °C twice at a heating or cooling rate of 10 °C/min.